Materials Research Express

PAPER

Safer modified Hummers' method for the synthesis of graphene oxide with high quality and high yield

Materials Research Express

RECEIVED
27 May 2019

REVISED
1 October 2019

ACCEPTED FOR PUBLICATION
10 October 2019

PUBLISHED
29 January 2020

PAPER

Safer modified Hummers' method for the synthesis of graphene oxide with high quality and high yield

Guillermo Santamaría-Juárez[1], **Estela Gómez-Barojas**[1,5], **Enrique Quiroga-González**[2,5], **Enrique Sánchez-Mora**[2], **Mildred Quintana-Ruiz**[3] and **J Deisy Santamaría-Juárez**[4]

[1] Benemérita Universidad Autónoma de Puebla (CIDS, IC-BUAP). PO Box 196, 72000 Puebla, México
[2] Institute of Physics, BUAP. PO Box J-48, 72570 Puebla, México
[3] Institute of Physics, UASLP. 78290, San Luis Potosí, México
[4] Faculty of Chemical Engineering, BUAP. 72570, Puebla, México
[5] Authors to whom any correspondence should be addressed.

E-mail: egomez@ifuap.buap.mx **and** equiroga@ieee.org

Keywords: graphene oxide, Hummers' method, graphite, TEM, XPS, UV-Vis spectroscopy

Abstract

We report on an improved method for the synthesis of graphene oxide based on the modified Hummers' method proposed by Marcano *et al* Different steps of the process were optimized. First, the concentration of the reactants and the reaction conditions were optimized to improve the efficiency of the oxidation process of graphite. The Raman spectrum of the GO shows the typical D and G typical of graphite oxide materials. The contribution of the area under the band D to the total area is 98%, confirming that almost the whole graphene was oxidized (high oxidation yield). Furthermore, the quantification of the C 1s XPS spectrum of our GO nanosheets indicates that about 77 wt% of oxygen in the form of oxygenated groups is bonded to the carbon nanosheets. Second, the reaction time was minimized to 12 h, without compromising the quality (as confirmed by micrography). Third, the production of toxic gases has been reduced. Fourth, a thermal treatment was introduced instead of the vacuum drying procedure traditionally used, greatly diminishing the overall graphite oxide processing time that includes: the reactant preparation, graphite oxidation process, rinsing and dispersion procedures, and drying (the drying time went from 12 h to 2 h). Reducing the total time by a half, compared to other methods, is an important finding considering scaling for industrial production.

1. Introduction

During the last decade, graphene, a monolayer one-atom-thick planar sheet of sp^2 hybridized carbon atoms densely packed in a honeycomb crystal lattice [1], has gained considerable interest because of its possible potential use as multifunctional material and wide range of applications in different kind of devices [2, 3] . In this regard, although the originally reported approach to the preparation of graphene (i.e. micromechanical cleavage of bulk graphite) leads to high-quality 2D crystals and is suitable for fundamental studies, it suffers from extremely low productivity and is therefore inadequate for large-scale use [4]. However, graphene has emerged as a material with high potential due to its remarkable properties such as high surface area, transparency [5], thermal conductivity [6] and good interface contact with adsorbents [7–9], etc.

As with any new material that is intended for large-scale applications for example in the areas: analog electronics and photonics/optoelectronics [10, 11], the development, and optimization of methods that allow the mass production and processing of graphene sheets is a top priority. At present, the only route that affords graphene-based sheets in considerable quantities relies on the chemical conversion of graphite into graphite oxide. Graphite oxide often called graphitic acid or graphitic oxide is a polycyclic aromatic hydrocarbon oxide interrupted by epoxides, alcohols, ketone carbonyls, and carboxylic groups [12–14].

According to Hontoria *et al* [15, 16] this disruption of the lattice is reflected in an increase of interlayer space from 0.335 nm for graphite to more than 0.65 nm for graphite oxide layers. The oxygen functional groups

convert the graphite oxide into a hydrophilic character; then; graphite oxide can be exfoliated in many polar solvents and dispersed particularly well in water [17–19]. The graphite oxidation processes via strong oxidants produce graphite oxide nanosheets with different oxygen-containing functional groups and defects [14]. Brodie *et al* [20–22] first demonstrated the synthesis of graphite oxide in 1859 by adding a portion of potassium chlorate ($KClO_3$) to slurry of graphite in fuming nitric (HNO_3) acid. The product they obtained was insoluble in acids and saline solutions, but it was soluble in pure water and in alkalis; in comparison to other graphite oxides, this product was more difficult to purify. They found that this product contained: the elements of sulfuric acid (H_2SO_4) combined with oxygen, hydrogen and a large amount of carbon. In 1898, Staudenmaier improved Brodie's method by replacing about two-thirds of fuming nitric acid (HNO_3) by concentrated H_2SO_4 enhancing the acidity in the mixture and added $KClO_3$ to oxidize the graphite in nitric acid, minimizing in this way the risk of explosion [23–25]. It was until 1909, that Charpy developed a method using the potassium permanganate ($KMnO_4$) as the oxidant agent to oxidize the graphite in H_2SO_4 at room temperature [26, 27].

The most important and widely used method for the synthesis of graphite oxide is the one developed by Hummers and Offeman in 1958 (Hummers' method) [28, 29]. This method includes all former developments but with key improvements. It consists of carrying out a reaction of graphite powder with $KMnO_4$ and $NaNO_3$ in concentrated H_2SO_4. They used H_2SO_4 to disperse graphite and a mixture of $KMnO_4$ and $NaNO_3$ as oxidant agent; the temperature was kept below 45 °C and the reaction time was just a few minutes long. Basically, the reaction took place in an acid solution and the addition of hydrogen peroxide (H_2O_2) made easier to remove the metal salts.

In general, all methods mentioned above produce explosive exothermic reactions and generate toxic gases such as NO_2, N_2O_4, and ClO_2 during the reaction; besides, residual Na^+ and NO_3 ions are difficult to be removed during the procedures of rinsing and purifying the graphite oxide. It was in 2010 that Marcano *et al* [30, 31] improved the Hummers' method by excluding $NaNO_3$, increasing the $KMnO_4$ oxidants, and performing the reaction in a mixture of H_2SO_4/H_3PO_4 in volume proportion 9:1. This modification was successful in increasing the reaction yield and reducing the toxic gases production. Later on, in 2013 Yeon-Ran Shin *et al* [32] returned to the idea of the first reports for producing graphite oxide, by observing that the optimized ratios of the H_2SO_4/HNO_3 mixture used in Hummers' method acted as a chemical 'scissor' and a chemical 'drill' in graphene planes to facilitate the penetration of the oxidant solution. However, the risk of explosion caused by HNO_3 was still present; this is why this acid was substituted by $KMnO_4$ [33]. Thus, a complete oxidation of graphite could be achieved using a mixture of $KMnO_4/H_2SO_4$ forming a graphite bisulfate product in which every single-layer of graphene is sandwiched by the layers of bisulfate ions [34, 35]. The complete intercalation of bisulfate ions ensures the effective infiltration of the $KMnO_4$ solution among the graphene layers for their surface oxidation.

The objective of this work is to optimize the steps of the graphite oxidation process such as: (1) reactants ratio following the Marcano *et al* [30] and Yeon-Ran *et al* [32] methods, (2) experimental conditions: reaction time and environmental parameters as temperature, pressure and stirring, in order to improve the efficiency of the oxidation process and reduce toxic gases reaction sub-products and (3) final product purification as rising and drying procedures. This optimization will allow increasing the amount of hydrophilic graphite oxide in less processing time. Moreover, different microscopic and spectroscopic techniques were used to analyze the shape, quality and oxidation degree of the synthesized graphite oxide sheets.

2. Materials and methods

2.1. Synthesis of graphite oxide

We started the synthesis of graphite oxide by using graphite powder (Bay carbon, spectroscope powders, Bay City, Michigan 48706, ~100 μm) and followed mainly Marcano *et al* [30] method because it produces graphene oxide sheets of good quality and does not use $NaNO_3$ as the oxidant to avoid the residual Na^+ and NO_3^- ions. Hummers *et al* [25, 36] and Nekahi *et al* [26, 37] used $KMnO_4$ as the oxidant agent to oxidize graphite and Drewniak *et al* [27, 38] used H_2SO_4 acid to improve the oxidation efficiency of $KMnO_4$. We have improved further the oxidation efficiency of $KMnO_4$ by adding H_3PO_4 to increase the acidity of the medium. Thus, we added a mixture of graphite and $KMnO_4$ powders (3:18 g; 3:6 wt%) into an H_2SO_4/H_3PO_4 solution (360:40 ml; 9:1 v/v%). One of the sub-products of the $KMnO_4$ and H_2SO_4 reaction is Mn_2O_7 which detonates at temperatures above 55 °C [22, 35]; thus to prevent an explosion we cooled down both mixtures before mixing them. Consequently, only a slightly exothermal reaction took place at 35 °C–40 °C and the solution turned purple-brown color. Next, the mixture was heated at 50 °C with continuous stirring for 12 h. At this point the mixture turned dark brown indicating that the graphite oxidation reaction already took place. During this thermal process the mixture undergoes remarkable changes: gases are given off from the interior of the substance, which swells up the system in a most singular manner separating the carbonaceous sheets and

Table 1. Reaction conditions for the oxidation of graphite.

Method	Reactants						Reaction	References
	Graphite (g)	$NaNO_3$ (ml)	$KMnO_4$ (g)	$Na_2Cr_2O_7$ (g)	H_2SO_4 (ml)	H_3PO_4 (ml)		
Chandra *et al*	1	—	—	4	15	—	72	[43]
Nekahi *et al*	1	15	3	—	20	—	24	[37]
Drewniak *et al*	1	3 g	3	—	30	—	2	[38]
Hummers *et al*	1	0.5 g	3	—	22.5	—	0.5	[28]
Marcano *et al*	3	—	18	—	360	40	16	[30]
This work	3	—	18	—	360	40	12	

reducing them to the minutest state of division which have the appearance and the structure of lamellar graphite [16, 20], larger surface areas of the carbonaceous sheets are in contact with the $KMnO_4$ increasing their oxidation state.

The chemical reaction that takes place during the thermal process is shown in equation (1). The oxidation of graphite by potassium permanganate ($KMnO_4$) is usually a multi–stage process. The reaction of $KMnO_4$ with sulfuric acid (H_2SO_4) produces diamanganese heptoxide (Mn_2O_7) being this the active species to oxidize graphite. The Mn_2O_7 is far more reactive than its monometallic tetraoxide (MnO_4^-) counterpart and it is known that Mn_2O_7 detonates when heated to temperatures greater than 55 °C or when placed in contact with organic compounds [39–41]. The reduction in the permanganate ions (MnO_4^-) to an oxidation manganate state has been reported in alkaline pH aqueous systems and it is considered to be responsible for an alkane oxidation reaction decrease [33]. The oxidizing power of the permanganate anions decreased remarkably in the order of $(MnO_4)^{-}$>$(MnO_4)^{2-}$>$(MnO_4)^{3-}$ [40]. Tromel and Russ demonstrated the ability of Mn_2O_7 to selectively oxidize unsaturated aliphatic double bonds over aromatic double bonds, which may have important implications for the structure of graphite and reaction pathway(s) occurring during the oxidation. [33, 42].

$$KMnO_4 + 3H_2SO_4 \rightarrow K^+ + MnO_3^+ + H_3O^+ + 3HSO_4 \rightarrow MnO_3^+ + MnO_4^- \rightarrow Mn_2O_7 \quad (1)$$

Based on these experimental results we infer that 12 h of the oxidation process is the appropriate time in which an efficient graphite oxidation reaction takes place. We highlight that 12 h of the graphite oxidation process is 73% shorter than 72 h used by Chandra *et al* [43] and 50% shorter than 24 h used by Nekahi *et al* [37]. Reaction times shorter than 12 h produce inefficient graphite oxidation processes [28, 38, 44, 45]. For comparison, in table 1 we list the reaction conditions, reactants and reaction times used in the different modified versions of the Hummers' method.

As can be seen from the table 1, we avoided the use of $NaNO_3$ to minimize the evolution of toxic gases, and reduced the processing time used by Marcano *et al* [30]. According to the literature, Hummers *et al* [36], Hummers and Offeman [28], Nekahi *et al* [37] and Drewniak *et al* [38] used H_2SO_4 to disperse graphite, and a mixture of $KMnO_4$ and $NaNO_3$ as oxidant agents. All these methods produce explosive exothermic reactions and generate toxic gases such as NO_2 and N_2O_4 besides, residual Na^+ and $^-NO_3$ ions are difficult to be removed during the procedures of rinsing and purifying the graphite oxide. Since we did not use $NaNO_3$ as oxidant agent, the reaction produces no toxic gases such as the ones mention above. The reaction between H_2SO_4 and $KMnO_4$ as oxidant agent is a dissociation given by equation (1). Continuing with the rinsing procedure, the mixture was let cool down to room temperature, afterwards 400 ml of DI water in ice form was added to decrease its viscosity and avoid overheating [46, 47]. Later on, 9 ml of H_2O_2 (H_2O_2/DI water, 30% v/v) was added to the mixture to make easier the removal of metal salts such as permanganate and manganese residuals from the mixture, now this solution turned to a bright yellow color. The solution was centrifuged at 1500 rpm for one hour and the supernatant decanted away. The remainder was repeatedly rinsed in continuous succession with: (1) 200 ml of DI water, (2) 200 ml of HCl at 30% v/v and (3) 200 ml of ethanol to remove the byproducts (e.g., potassium-containing compounds) that can cause an acute explosion [36, 48]; after each rinsing step, the solution was centrifuged at 4000 rpm for 2 h and the supernatant decanted away. Then, the remainder obtained after the rinsing procedure was coagulated with 40 ml of ether. Later on, the resulting suspension was filtered through a PTFE membrane with 0.45 μm pore size.

The solid material obtained on the filter was vacuum-dried for overnight at room temperature. To remove left over water from graphite oxide, we carried out a thermal treatment at 60 °C under nitrogen flux for 2 h. The temperature of 60 °C was chosen because in the range from 30 °C to 150 °C no chemical reactions take place, but only an evaporation of the solvents contained on the graphene sheets is carried out; therefore, only a mass loss is observed as indicated by the thermograms of GO performed by Michael J. McAllister *et al* in 2007 [49] and Cheng-Meng Chen *et al* in 2012 [50]. Besides, at 60 °C the evaporation is relatively slow, preventing any structural damage. The nitrogen flux prevents any reflux, decreasing the time for the drying process. The final

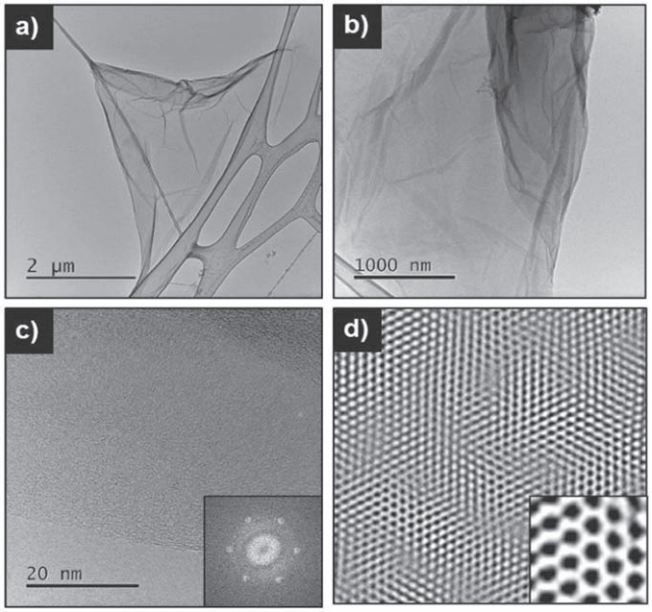

Figure 1. Observations of GO sheets in a TEM microscope: (a) and (b) TEM micrograph, (**c**) HRTEM, with the inset presenting the SAED pattern of this area, and (d) FFT of the SAED pattern.

product in powder form weighted 6.8 g. By considering a graphite initial weight of 3 g, it is estimated that about 80% of carbon is linked to oxygen in different ways, including $^{-}$OH groups.

It is already known that chemically both graphite oxide and graphene oxide (GO) have similar or identical structures. Both possess stacked structures with chemical functionality on their basal planes and at their edges [33]. The only difference between them is the number of stacked layers; GO possesses a monolayer or just a few stacked layers, while graphite oxide contains a greater number of stacked layers [33, 51]. Taking into account that the formation of oxygenated functional groups in graphite oxide makes them easier to exfoliate it into monolayers of GO, we dispersed 1 mg of graphite oxide powder in 100 ml DI water by sonication for 10 min to obtain GO nanosheets. Then, the prepared samples were analyzed by microscopic and spectroscopic techniques.

2.2. Characterization techniques

The surface morphology of the GO samples was analyzed using a high-resolution transmission electron microscope (HRTEM) JEOL JEM-2100F operated at 200 kV acceleration voltage. The FTIR spectrum (400–2000 cm^{-1}) was measured by means of a Spectrum One Perkin Elmer system with an ATR accessory and at 8 nm s^{-1} scan velocity. Raman spectra were recorded with a Raman Scientific XRD, Thermo SCIENTIFIC system with a He-Ne laser ($\lambda = 632.8$ nm) as the excitation source and 10 mW of power. The entrance and exit slits aperture was 50 μm. Also, an optic microscope is coupled to this system. 10X magnification was used to select the region of interest. X-ray Photoelectron Spectroscopy (XPS) system K-Alpha + Thermo Scientific, with a Constant Analyzer Energy (CAE), was used to investigate the state of elements present in the graphite oxide. XPS spectra were obtained by irradiating the sample with the beam of x-ray, Al K_α (1486.6 eV). The primary beam energy of 12 kV and primary current of 6 mA were used, operating at pass energy of 0.2 eV. The pressure in the analysis chamber was 2×10^{-9} Torr. XPS gives quantitative information about chemical groups and the chemical shift in XPS is a measure of the valence charge on the atom of interest.

3. Results

3.1. Morphological and structural characterization

The surface morphology and crystallinity of synthesized graphite oxide was analyzed by means of an HRTEM and selected area electron diffraction (SAED). Figures 1(a), (b) shows TEM micrographs of graphite oxide previously dispersed in DI water by sonication and set on a Carbon/Nickel holder for characterization. Figure 1(a) shows a representative TEM micrograph of a GO sheet, it shows and average size of ~2 $\pm$ 0.2 μm. It can be observed that the morphology of GO is sheet-like; the sheets look translucent, well defined with some wrinkles on the surface and with no folding on the edges. In these micrographs, dark and light zones and some

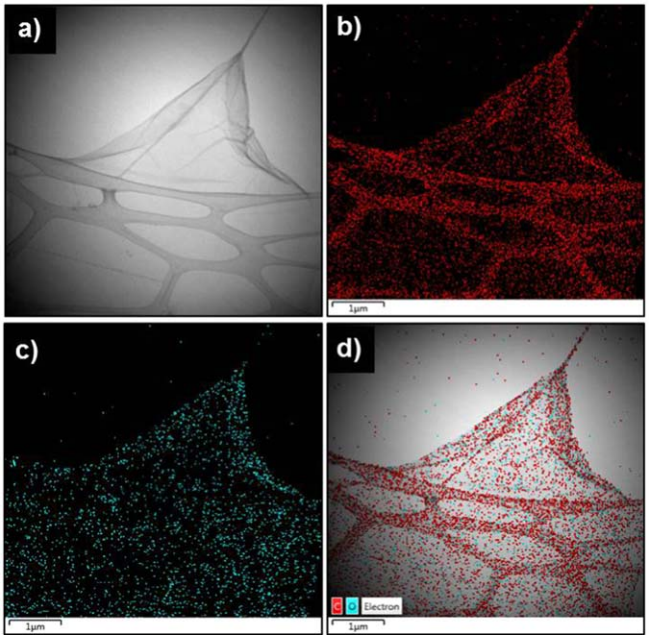

Figure 2. (a) A TEM micrograph of the surface morphology of a GO sheet. EDS compositional maps: (b) carbon, (c) oxygen and (d) an overlay of carbon and oxygen maps.

imperfections like dark points on the surface can be observed. They are related to the existence of carbon atoms with sp^3 hybridization that constitute the hydroxyl or epoxy groups in the GO sheet.

Figure 1(c) shows an HRTEM image of the GO nanolayer and in the inset its corresponding SAED pattern. In the SAED pattern clear diffraction spots are observed; by applying the Fast Fourier Transform (FFT) to the SAED pattern, the Moiré pattern with the hexagonal lattice structure formed by carbon atoms is revealed as shown in figure 1(d); for a better visualization a magnification of the lattice is shown in the inset.

Furthermore, the GO nanolayer was analyzed by Energy Dispersive Spectroscopy (EDS). Figure 2(a) shows the GO nanosheet set on the Carbon/Nickel holder. The bands in this figure correspond to the grid that holds the sample. EDS mapping images are shown: in (b) carbon in red, (c) oxygen in blue and (d) the overlay of the two maps; in this image we observe the distribution of the Carbon and Oxygen chemical elements constituting the GO nanosheets.

3.2. FTIR spectroscopy

Figure 3 shows an FTIR transmission spectrum recorded with ATR accessory from GO in the range from 4000 to 700 cm^{-1}. In this spectrum different peaks appear that are assigned to vibrational modes of functional oxygen-containing groups; for a better visualization see points (A), (B) and (C) on the inset of this figure. Additionally, C=C vibrations of graphene and C–O vibrations of GO are also present, as expected.

In table 2 the measured peaks positions, the reported ones, and their assignments according to the literature are listed. There is a good concordance between the two groups. We infer then, that the GO nanosheets are covered by functional groups such as hydroxyl (–OH), epoxy (C–O–C) and carboxylic (–COOH) groups. It is worthwhile to mention that the FTIR spectrum of GO recorded after one year is very similar to the one recorded from fresh GO, this means that GO is stable with respect to aging.

3.3. Raman spectroscopy

Raman spectroscopy is commonly used to investigate the microstructure and perfectness of carbon-based materials. The main Raman parameters to be evaluated are the peak position, Full Width at Half Maximum (FWHM), intensity ratio of the bands peaks, and the total areas under the Raman curves. Figure 4 shows the Raman spectrum of GO in the range (750–3100 cm^{-1}). This spectrum can be divided into two regions: the first order effect region (750–2500 cm^{-1}) and the second order effect region (2500–3100 cm^{-1}) [59].

In the first order range, there appears the D band (the symmetry A_{1g} mode) at 1350 cm^{-1}. It corresponds to a defect-induced vibration mode or to vibrations caused by imperfections due to the attachment of functional groups to the graphitic carbon basal plane [59], such as the hydroxyl and epoxide groups. Other origins of this band have been attributed to a symmetry loss due to the finite size of graphite crystals [60], to stretching vibrations of carbon bonds with a sp^3 hybridization [60] or to breathing modes of the aromatic rings with free

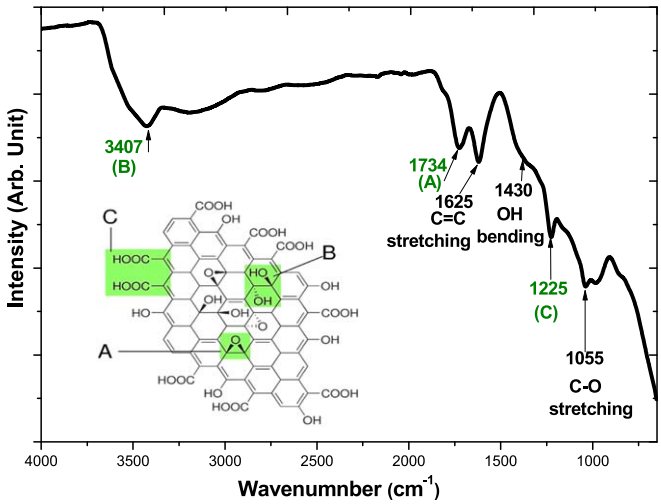

Figure 3. FTIR-ATR transmission spectrum of GO.

Table 2. GO vibrational modes assignments reported in the literature and measured.

Reported peak position (cm^{-1})	Measured peak position (cm^{-1})	Functional group	Vibration mode	References
3410	3407	Water (–OH)	Stretching	[52]
1734	1734	Carboxylates or Ketone (C=O)	Stretching	[53, 54]
1629	1625	Bonding C=C	Stretching	[55]
1420	1430	Alcohols (–OH)[a]	Bending	[56, 57]
1227	1225	Epoxide (C–O–C) or Phenols (C–O–H)	Stretching	[57, 58]
1055	1055	Bonding C–O	Stretching	[57, 58]

[a] Shoulder of bending OH.

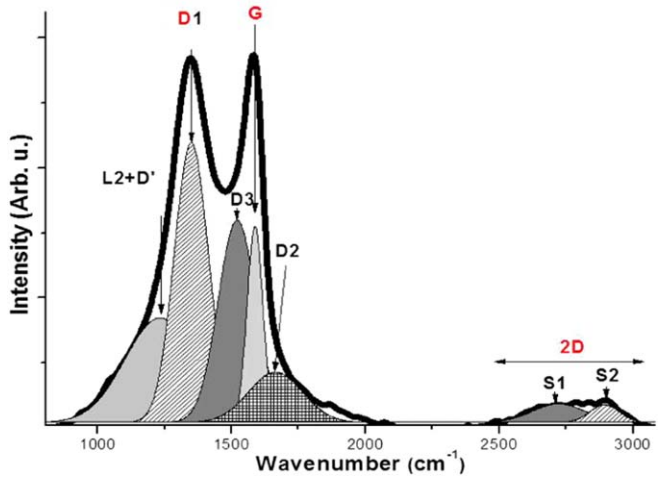

Figure 4. Raman spectrum of GO.

bonds in the plane terminations [61]. The G band (the E_{2g} mode of the sp^2 carbon atoms) at 1580 cm^{-1} is due to first order scattering E_{2g} mode of graphene [61, 62], that is, to vibrations inside the aromatic layers of the graphite structure, see figure 4.

The D band in figure 4 has been fitted by a sum of two Gaussian bands centered at 1233 cm^{-1} (L2 + D′) and 1350 cm^{-1} (D1) and the G band by a sum of three Gaussian bands centered at 1521 cm^{-1} (D3), 1580 cm^{-1} (G) and 1632 cm^{-1} (D2). Double resonance can also happen as an intravalley process that is, connecting two points belonging to the same cone around K (or K′). This gives the so-called D′ peak. The 2D peak is the D-peak

Table 3. Intensity and areas of the main and secondary Raman bands.

Band	Theoretical position (cm^{-1})	Experimental position (cm^{-1})	FWHM (nm)	Intensity (Arb. units)	Area (Arb. units)
L2 + D′	1230	1233	263	402	132 337
D_1	1350	1348	241	1347	380 698
D_3	1578	1580	159	754	55 466
G	1580	1579	123	766	11 092
D_2	1635	1632	210	143	37 573
S_1	2700	2701	183	65	14 863
S_2	2900	2898	100	62	7813

overtone, and the 2D′ peak is the D′ overtone. Because the 2D and 2D′ peaks originate from a process where momentum conservation is satisfied by two phonons with opposite wave vectors, no defects are required for their activation, and are thus always present.

The band L2 + D′ is the product of overtones of the D2 band and the interactions of optical longitudinal and acoustic vibrations [63]. The peak D1 is intense, wide, and it belongs to carbonaceous materials with disordered structure, attributed to in-plane defects like heteroatoms (O, H, N for instance) or structural defects. Its peak position depends on wavelength of the incident laser [64]. The integral of D1 is small when the aromatic planes are ordered and this band gets more intense and wide when there exist some defects in graphite [65]. The D3 band is attributed to a disordered carbonaceous material containing out of plane defects like tetrahedral carbon atoms, organic molecules, and functional groups, and it is absent in samples having undergone thermal treatments at a temperature higher than 450 °C [65]. The D2 band (also named D′) at about 1635 cm^{-1} is due to the non-homogeneity or deformation of the material [66].

In the second order range the 2D band appears, which is wide and of low intensity and it is composed of S1 and S2 sub-bands. The S1 band at 1350 cm^{-1} is considered by Stephanie *et al* as an overtone of D1 [61]. The S2 band at 2900 cm^{-1} appears only on graphitic materials as a consequence of C-H bonding [64]. This band has also been interpreted as the combination of the D and G bands [67].

The D and G bands of GO differ from those of graphite in three aspects: 1) a significant increase in the D/G intensity ratio (I_D/I_G) associated to a disruption of the lattice symmetry; 2) broadening of both the D and G bands associated with the introduction of hydroxyl and epoxy groups and 3) shifts of the D and G bands towards higher wavenumbers are related to an increase of isolated carbon double bonds in GO [15]. This is why it is difficult to use the ratio I_D/I_G as an indicative of pureness or graphitic level of GO. Instead, Beyssac *et al* [64] have proposed other figures of merit calculated as the ratio of areas under the bands, in order to estimate the carbonaceous material (CM) degree of organization. They defined the ratio of areas R2 = D1/(D1 + G + D2). The authors excluded D2 from R2 because the D2 band corresponds to poorly ordered carbons and to out-plane defects like tetrahedral carbons that, as Beny-Bassez *et al* [65] suggest, are released early during the graphitization process at high temperatures as happens in mineral graphite. It is worthy of mention that the figure of merit was proposed for mineral graphite, where the most representative D band is D1, thus, in that case, R2 gets the form, R2′ = D1/(D1 + G). For poorly organized CM, R2′ is greater than 0.5, while in CM well organized R2′ smaller than 0.5. It is important to take into account that he spectra measured at the surface exhibit a higher contribution of the defect bands (D1 and D2) [66, 67]. For the GO produced in this work, the bands D1, D2, and D3 appear due to the low-temperature synthesis process and it is better to consider the areas ratio R′ = (D1 + D2 + D3)/(D1 + D2 + D3 + G) i.e. the ratio of modes from defects (non-graphitic modes) to the total modes. From data in table 3, it was possible to calculate R′, which gives a value of 0.98. Such a high value may indicate that almost the whole graphene was oxidized. The sp^1 bonds (and deformations) produced by the oxidation of the carbon sheets give rise to the D band. However, certain graphitic level is still present inferred by the presence of the G band indicating that GO is not just in the form of monolayers.

3.4. XPS

The chemical state of the GO was analyzed by XPS. Figure 5 shows the two most prominent bands of GO: (a) spectrum of the C 1s (FWHM = 4.77 eV) and (b) the O 1s spectrum (FWHM = 2.04 eV).

The C 1s in the XPS spectrum shows 5 components assigned to binding energies of: C=C (284.8 eV, FWHM = 1.5 eV), C–C (285.4 eV, FWHM = 2.29 eV), C–O (287.1 eV, FWHM = 2.12 eV), C=O (287.7 eV, FWHM = 1.92 eV) and O=C–OH (289.2 eV, FWHM = 2.3 eV) [33, 40, 68, 69]. The presence of these groups suggests a considerable degree of oxidation of the GO nanosheet [47]. This last assumption is confirmed by the position of the O 1s band, which is in the range of carbon-oxygen bonds.

The quantification of the XPS spectrum of our graphene nanosheets is: 56.2 wt% of C and 42.9 wt% of O, and the elements N and S wt% values correspond to trace impurities in the nanosheets. These C and O

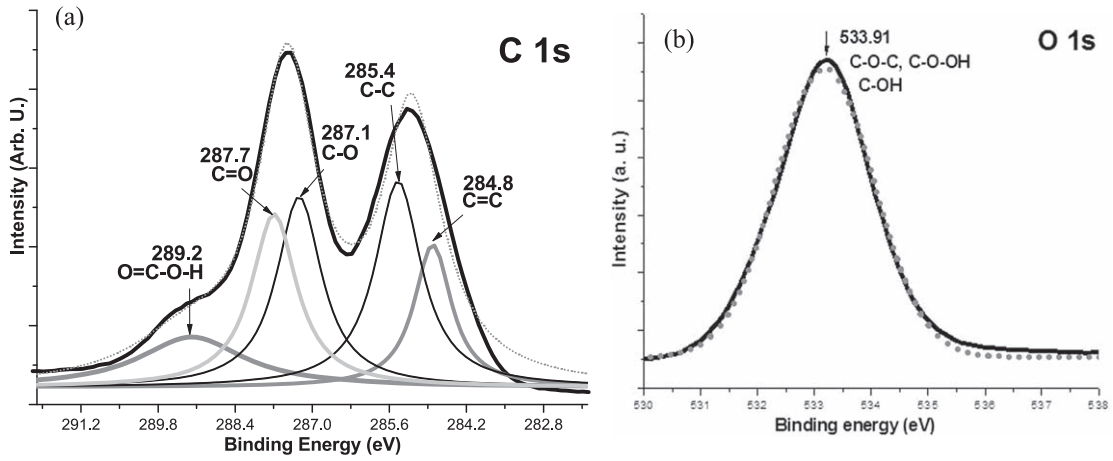

Figure 5. XPS spectra of GO: (a) C 1s and (b) O 1s.

Table 4. Elemental composition of graphite oxide obtained by different Hummers' modified methods [44].

Sample	Elemental analysis (wt%)			
	C	N	S	O
Chandra *et al*	75.97	0.10	2.53	21.40
Nekahi *et al*	59.17	0.10	0.10	40.63
Drewniak *et al*	57.19	0.10	0.30	42.41
Hummers *et al*	65.71	0.10	0.61	33.58
This work	56.2	0.20	0.70	42.90

percentages mean that about 77 wt% of oxygen in the form of oxygenated groups is bonded to the carbon nanosheets; thus, the process has a high oxidation yield. In table 4 the elemental composition of the here produced GO is compared with the composition of the GO prepared by other chemical methods, reported in [44]. It is important to mention that the data of the reference was obtained from CHNOS elemental analysis.

In the oxidation route of Chandra, the treatment with sodium dichromate provided the lowest oxygen content (21.40 wt%) even with very long reaction time (72 h). The Hummers' method gave 33.58 wt% of O in 0.5 h of reaction time. The Nekahi *et al* and Drewniak *et al* graphite oxidation methods provided about the same oxygen weight percentage, being the sample of Drewniak *et al* the one with the highest O content (42.41 wt%). We obtained a slightly higher O percentage (42.9 wt%), see table 4. In conclusion, our GO presents the highest degree of oxidation. Moreover, a highlight of our process is that we excluded the use of the $NaNO_3$ reactant, minimizing the production of toxic gases.

4. Conclusions

Increasing the amount of $KMnO_4$, excluding the $NaNO_3$ and adding a mixture of H_2SO_4/H_3PO_4 in proportion 9:1, the efficiency of the oxidation process of the graphite has been improved compared with the method that uses $KMnO_4$, $NaNO_3$, and H_2SO_4 for preparing GO. With the present method, no toxic gases are generated, and it results in a higher amount of hydrophilic oxidized graphene material. By carrying out a thermal treatment in an oven at low temperature and under nitrogen flux, the drying procedure time has been greatly reduced and graphite oxide has not been reduced. TEM micrographs indicated that the GO sheets are translucent and wrinkled. SAED patterns reveal the hexagonal lattice structure of carbon atoms. EDS mappings show the distribution of Carbon and Oxygen in the GO nanosheets. By FTIR characterization it was possible to identify the functional oxygen-containing groups. Raman spectra of the synthesized GO showed the D and G Raman bands typical of graphite oxide materials. The deconvolution of these bands revealed the secondary Raman bands: D1, D2 and D3 which indicate the disordered structure of carbonaceous materials, most probably due to the oxidation of graphite. This inference is confirmed by the presence of the 2D band. The proportions of the areas under the curves of the G and D bands indicate that the GO nanosheets are almost completely oxidized. The deconvolution of the C 1s XPS spectrum reveals the 3 different carbon bonds in GO, suggesting a

considerable oxidation degree of the GO nanosheets. The main conclusion of this work based on the characterization results shown above is that the optimization of the graphite oxidation process performed in this work produces GO nanosheets of good quality in a high yield.

Acknowledgments

This work has been partially supported by CONACYT through a graduate student scholarship and by SEP-IFUAP- 'Low Dimensional Structures' research group (CA-315).

ORCID iDs

Estela Gómez-Barojas https://orcid.org/0000-0001-8998-1148

References

[1] Wu J-B, Lin M-L, Cong X, Liu H-N and Tan P-H 2018 Raman spectroscopy of graphene-based materials and its applications in related device *Chem. Soc. Rev.* **47** 1822–73
[2] Xie C, Wang Y, Zhang Z-X, Wang D and Luo L B 2018 Graphene/semiconductor hybrid heterostructures for optoelectronic device applications *Nano Today* **19** 41–83
[3] Maitra A, Das A K, Bera R, Karan S K, Paria S, Si S K and Khatua B B 2017 An approach to fabricate PDMS encapsulated all-solid-state advanced asymmetric supercapacitor device with vertically aligned hierarchical Zn–Fe–Co ternary oxide nanowire and nitrogen doped graphene nanosheet for high power device applications *ACS Appl. Mater. Interfaces* **9** 5947–58
[4] Peng L, Xu Z, Liu Z, Wei Y, Sun H, Li Z, Zhao X and Gao C 2015 An iron-based green approach to 1-h production of single-layer graphene oxide *Nat. Commun.* **6** 5716
[5] Qi Y *et al* 2018 Switching vertical to horizontal graphene growth using faraday cage-assisted PECVD approach for high-performance transparent heating device *Adv. Mater.* **30** 1704839
[6] Ma T, Gao H-L, Cong H-P, Yao H-B, Wu L, Yu Z-Y, Chen S-M and Yu S-H 2018 A bioinspired interface design for improving the strength and electrical conductivity of graphene-based fibers *Adv. Mater.* **30** 1706435
[7] Lu S-Y, Jin M, Zhang Y, Niu Y-B, Gao J-C and Li C M 2017 Chemically exfoliating biomass into a graphene-like porous active carbon with rational pore structure, good conductivity, and large surface area for high-performance supercapacitors *Adv. Energy Mater.* **8** 1702545
[8] Kyzas George Z, Deliyanni E A, Bikiaris D N and Mitropoulos A C 2018 Graphene composites as dye adsorbents: review *Chem. Eng. Res. Des.* **129** 75–88
[9] Gamze Ersan O G, Apul F and Perreault T K 2017 Adsorption of organic contaminants by graphene nanosheets: a review *Water Res.* **126** 385–98
[10] Ricciardulli A G, Yang S, Wetzelaer G - J A H, Feng X and Blom P W M 2018 Hybrid silver nanowire and graphene-based solution-processed transparent electrode for organic optoelectronics *Adv. Funct. Mater.* **28** 1706010
[11] Liang F-X, Gao Y, Xie C, Tong X-W, Li Z-J and Luo L-B 2019 Recent advances in the fabrication of graphene–ZnO heterojunctions for optoelectronic device applications *J. Mater. Chem.* C **6** 3815–33
[12] Yang Z *et al* 2019 Long-term antibacterial stable reduced graphene oxide nanocomposites loaded with cuprous oxide nanoparticles *J. Colloid Interface Sci.* **533** 13–23
[13] Mei Q, Liu B, Han G, Liu R, Han M-Y and Zhang Z 2019 Graphene oxide: from tunable structures to diverse luminescence behaviors *Adv. Sci.* **6** 1900855
[14] Lee X J, Hiew B Y Z, Lai K C, Lee L Y, Gan S, Thangalazhy-Gopakumar S and Rigby S 2019 Review on graphene and its derivatives: synthesis methods and potential industrial implementation *J. of the Taiwan Institute of Chemical Engineers* **98** 163–80
[15] Hontoria Lucas C, López Peinado A, López González J, Rojas Cervantes M and Martin Aranda R 1995 Study of oxygen-containing groups in a series of graphite oxides: physical and chemical characterization *J Carbon* **33** 1585–92
[16] Hu J 2013 Graphene-oxide-stabilized atomic Ti for H_2O_2 activation and propylene epoxidation: a first-principle study *J. Phys. Chem.* C **117** 16005–11
[17] Texter J 2014 Graphene dispersions *Current Opinion in Colloid & Interface Science* **19** 163–74
[18] Gudarzi M M . 2016 Colloidal stability of graphene oxide: aggregation in two dimensions *J. Langmuir* **32** 5058–68
[19] Ogino I, Yokoyama Y, Iwamura S and Mukai S R 2014 Exfoliation of graphite oxide in water without sonication: bridging length scales from nanosheets to macroscopic materials *Chem. Mater.* **26** 3334–9
[20] Brodie B C 1859 On the atomic weight of graphite *Philos. Trans. R. Soc. London* **149** 249–59
[21] Huitao Y, Bangwen Z, Chaoke B, Ruihong L and Ruiguang X 2016 High-efficient synthesis of graphene oxide based on improved Hummers method *Sci. Rep.* **6** 36143
[22] Pei S, Wei Q, Huang K, Cheng H-M and Ren W 2018 Green synthesis of graphene oxide by seconds timescale water electrolytic oxidation *Nat. Commun.* **9** 145
[23] Staudenmaier L 1898 Verfahren zur darstellung der graphitsäure *J. Ber. Dtsch. Chem. Ges.* **31** 1481–7
[24] Yoo M J and Park H B 2019 Effect of hydrogen peroxide on properties of graphene oxide in Hummers method *J. Carbon* **141** 515–22
[25] Al-Gaashani R, Najjarc A, Zakaria Y, Mansoura S and Atieh M A 2019 XPS and structural studies of high quality graphene oxide and reduced graphene oxide prepared by different chemical oxidation methods *Ceram. Int.* **45** 14439–48
[26] Charpy G 1909 Lur sar formation de l'oxyde graphitique et la définition du graphite *Comptes rendus hebdomadaires des séances de l'Académie des sciences* **148** 920–3
[27] Lowe S E and Zhong Y L 2017 Challenges of Industrial-Scale. Graphene Oxide Production *Graphene oxide: fundamentals and applications* ed Ayrat M. Dimiev and Siegfried Eigler First edn (New York: Wiley) 13 (https://doi.org/10.1002/9781119069447)
[28] Hummers W S and Offeman R E 1958 Preparation of graphitic oxide *J. Am Chem Soc* **80** 1339

[29] Paramasivan T, Sivarajasekar N, Muthusaravanan S, Subashini R, Prakashmaran J, Sivamani S and Ajmal Koya P 2019 Graphene family materials for the removal of pesticides from water *A New Generation Material Graphene: Applications in Water Technology* (Riyadh, Saudi Arabi: Springer International Publishing) **pp** 309–27
[30] Marcano D C, Kosynkin D V, Berlin J M, Sinitskii A, Sun Z and Slesarev A 2010 Improved synthesis of graphene oxide *ACS Nano* **4** 4806–14
[31] Husnah M, Fakhri H A, Rohman F, Aimon A H and Iskandar F 2017 A modified marcano method for improving electrical properties of reduced graphene oxide (rGO) *Mater. Res. Express* **6** 4
[32] Shin Y R, Jung S M, Jeon I Y and Baek J B 2013 The oxidation mechanism of highly ordered pyrolytic graphite in a nitric acid/sulfuric acid mixture *J. Carbon* **52** 493–8
[33] Dreyer D R, Park S, Bielawski C W and Ruoff R S 2010 The chemistry of graphene oxide *Chem. Soc. Rev.* **39** 228–40
[34] Avdeev V V, Monyakina L A, Nikolskaya I V, Sorokina N E and Semenenko K N 1992 The choice of oxidizers for graphite hydrogenosulfate chemical synthesis *J. Carbon* **30** 819–23
[35] Sorokina N E, Khaskov M A, Avdeev V V and Nikol'skaya I V 2005 Reaction of graphite with sulfuric acid in the presence of $KMnO_4$ *J. Russ. Gen. Chem.* **75** 162–8
[36] Hummers W S 1954 *US Patent No* 2 798 878(United States Patent Office)
[37] Nekahi A, Marashi P H and Haghshenas D 2014 Transparent conductive thin film of ultra large reduced graphene oxide monolayers *J. Applied Surface Science* **295** 59–65
[38] Drewniak S, Pustelny T and Muzyka R 2015 Investigations of selected physical properties of graphite oxide and thermally exfoliated/reduced graphene oxide in the aspect of their applications in photonic gas sensors *J. Photonics Letters of Poland* **7** 47–9
[39] Koch K R and Krause P F 1982 Oxidation by Mn_20_7: an impressive demonstration of the powerful oxidizing property of dimanganeseheptoxide *J. Chem. Ed.* **59** 973–4
[40] Ibarra-Hernández A, Vega-Rios A and Osuna V 2018 Synthesis of graphite oxide with different surface oxygen contents assisted microwave radiation *Nanomaterials* **8** 106
[41] Dash S, Patel S and Mishra B K 2008 Oxidation by permanganate: synthetic and mechanistic aspects *Tetrahedron* **65** 707–39
[42] Tromel M and Russ M 1987 Dimanganheptoxid zur selektiven oxidation organischer substrate *Angew. Chem* **99** 1037–8
[43] Chandra S, Sahu S and Pramanik P 2010 A novel synthesis of graphene by dichromate oxidation *J. Materials Science and Engineering* B **167** 133–6
[44] Roksana M, Kwoka M, Smędowski Ł, Díez N and Gryglewicz G 2017 Oxidation of graphite by different modified Hummers methods *J. New Carbon Materials* **32** 15–20
[45] Glemser V O and Schröder H 1953 Über manganoxyde: II. Zur Kenntnis des Mangan (VII)-oxyds *J. Chem* **271** 293–304
[46] Wang P, Wang J, Ming T, Wang X, Yu H, Yu J, Wang Y and Lei M 2013 Dye-sensitization-induced visible-light reduction of graphene oxide for the enhanced TiO_2 photocatalytic performance *ACS Applied Materials & Interfaces* **5** 2924–9
[47] Graeme W, Brian S and Prashant V K 2008 TiO_2-graphene nanocomposites UV-assisted photocatalytic reduction of graphene oxide 2008 *ACS Nano* **2** 1487–91
[48] Poh H L, Sanek F and Ambrosi A 2012 Graphenes prepared by staudenmaier, hofmann and Hummers methods with consequent thermal exfoliation exhibit very different electrochemical properties *J. Nanoscale* **4** 3515–22
[49] McAllister M J *et al* 2007 Single sheet functionalized graphene by oxidation and thermal expansion of graphite *Chem. Mater.* **19** 4396–404
[50] Chen C-M, Zhang Q, Yang M-G, Huang C-H, Yang Y-G and Wang M-Z 2012 Structural evolution during annealing of thermally reduced graphene nanosheets for application in supercapacitors *Carbon* **50** 3572–84
[51] Kim J, Cote L J, Kim F, Yuan W, Shull K R and Huang J 2010 Graphene oxide sheets at interfaces *J. Am. Chem. Soc* **132** 8180–6
[52] Paronyan T M 2017 Incommensurate graphene foam as a high capacity lithium intercalation anode *J Sci Rep* **7** 39944
[53] Shen J, Li T, Long Y, Shi M, Li N and Ye M 2012 One-step solid state preparation of reduced graphene oxide *J. Carbon* **50** 2134–40
[54] Li Q, Guo B, Yu J, Ran J, Zhang B, Yan H and Gong J 2011 Highly efficient visible-light-driven photocatalytic hydrogen production of CdS-cluster-decorated graphene nanosheets *J. Am. Chem Soc* **133** 10878
[55] Kuila T, Bose S, Khanra P, Mishra A K, Kim N H and Lee J H 2012 A green approach for the reduction of graphene oxide by wild carrot root *J. Carbon* **50** 914
[56] Zhang M, Qu B, Lei D, Chen Y, Yu X, Chen L, Li Q, Wang Y and Wang T J 2012 A green and fast strategy for the scalable synthesis of Fe_2O_3/graphene with significantly enhanced Li-ion storage properties *J. Mater. Chem.* **22** 3868
[57] Hou C, Zhang Q, Li Y and Wang H 2012 P25–graphene hydrogels: room-temperature synthesis and application for removal of methylene blue from aqueous solution *J. Hazard. Mater.* **205** 229–35
[58] Luo D, Zhang G, Liu J and Sun X 2011 Evaluation criteria for reduced graphene oxide *J. Phys. Chem.* **115** 11327
[59] Tuinstra F and Koenig J L 1970 Raman spectrum of graphite *J. Chem Physics* **53** 1126–30
[60] Roubin P, Martin C, Arnasa C, Colomban P, Pégouriéc B and Brosset C 2005 Raman spectroscopy and X-ray diffraction studies of some deposited carbon layers in Tore Supra *J. of Nuclear Materials* **337** 990–4
[61] Reich S and Thomsen C 2004 Raman spectroscopy of graphite *Phil. Trans. R. Soc. Lond.* **362** 2271–88
[62] Nagaveni K, Hegde M S, Ravishankar N, Subbanna G N and Giridhar M 2004 Synthesis and structure of nanocrystalline TiO_2 with lower band gap showing high photocatalytic activity *Langmuir* **20** 2900–7
[63] Ferrari1 A C and Basko D M 2013 Raman spectroscopy as a versatile tool for studying the properties of graphene *Nat. Nanotechnol.* **8** 235–46
[64] Beyssac G B, Chopin C and Rouzaud J N 2002 Raman spectra of carbonaceous material in metasediments: a new geothermometer *J. Metamorphic Geol* **20** 859–71
[65] Beny Bassez C and Rouzauo J N 1985 Characterization of carbonaceous materials by correlated electron and optical microscopy and raman microspectroscopy *Scanning Elec. Micros.* **1** 119–32
[66] Pasteris J D and Wopenka B 2004 Necessary, but not sufficient: Raman identification of disordered carbon as a signature of ancient life *Astrobiology* **3** 727–38
[67] Lee S-Y and Zhang D 2004 Theory of femtosecond stimulated Raman spectroscopy *J. of Chem. Phys.* **121** 3632
[68] Rabchinskii M K *et al* 2018 Facile reduction of graphene oxide suspensions and films using glass wafers *Sci. Rep.* **8** 14154
[69] Perera S D *et al* 2012 Alkaline deoxygenated graphene oxide for supercapacitor applications: an effective green alternative for chemically reduced graphene *J. Power Sources* **215** 1–10